applied sciences

MDPI

Article

Influence of Oxygen Admixture on Plasma Nitrocarburizing Process and Monitoring of an Active Screen Plasma Treatment

Jan Böcker [1,*], Anke Dalke [1,*], Alexander Puth [2,3], Christian Schimpf [4], Jürgen Röpcke [2], Jean-Pierre H. van Helden [2] and Horst Biermann [1]

1 Institute of Materials Engineering, Technische Universität Bergakademie Freiberg, Gustav-Zeuner-Straße 5, 09599 Freiberg, Germany; biermann@ww.tu-freiberg.de
2 Leibniz Institute for Plasma Science and Technology (INP), Felix-Hausdorff-Straße 2, 17489 Greifswald, Germany; a.d.f.puth@tue.nl (A.P.); roepcke@inp-greifswald.de (J.R.); jean-pierre.vanhelden@inp-greifswald.de (J.-P.H.v.H.)
3 Department of Applied Physics, Eindhoven University of Technology, Postbus 513, 5600 MB Eindhoven, The Netherlands
4 Institute of Materials Science, Technische Universität Bergakademie Freiberg, Gustav-Zeuner-Straße 5, 09599 Freiberg, Germany; schimpf@iww.tu-freiberg.de
* Correspondence: jan.boecker@iwt.tu-freiberg.de (J.B.); dalke@ww.tu-freiberg.de (A.D.); Tel.: +49-(0)3731-39-2392 (J.B.); +49-(0)3731-39-2685 (A.D.)

Abstract: The effect of a controlled oxygen admixture to a plasma nitrocarburizing process using active screen technology and an active screen made of carbon was investigated to control the carburizing potential within the plasma-assisted process. Laser absorption spectroscopy was used to determine the resulting process gas composition at different levels of oxygen admixture using O_2 and CO_2, respectively, as well as the long-term trends of the concentration of major reaction products over the duration of a material treatment of ARMCO® iron. The short-term studies of the resulting process gas composition, as a function of oxygen addition to the process feed gases N_2 and H_2, showed that a stepwise increase in oxygen addition led to the formation of oxygen-containing species, such as CO, CO_2, and H_2O, and to a significant decrease in the concentrations of hydrocarbons and HCN. Despite increased oxygen concentration within the process gas, no oxygen enrichment was observed in the compound layer of ARMCO® iron; however, the diffusion depth of nitrogen and carbon increased significantly. Increasing the local nitrogen concentration changed the stoichiometry of the ε-$Fe_3(N,C)_{1+x}$ phase in the compound layer and opens up additional degrees of freedom for improved process control.

Keywords: active screen technology; plasma nitrocarburizing; process monitoring; gas diagnostics; laser absorption spectroscopy; compound layer; oxygen

Citation: Böcker, J.; Dalke, A.; Puth, A.; Schimpf, C.; Röpcke, J.; van Helden, J.-P.H.; Biermann, H. Influence of Oxygen Admixture on Plasma Nitrocarburizing Process and Monitoring of an Active Screen Plasma Treatment. *Appl. Sci.* **2021**, *11*, 9918. https://doi.org/10.3390/app11219918

Academic Editors: Gabriele Cristoforetti and Vincenzo Palleschi

Received: 21 September 2021
Accepted: 21 October 2021
Published: 23 October 2021

1. Introduction

Plasma nitrocarburizing (PNC) is an industrially established process applied in order to improve corrosion resistance and fatigue behavior, as well as the wear resistance of engineering materials like plain carbon or tool steels [1]. The production of thick compound layers consisting of the ε-$Fe_3(N,C)_{1+x}$ phase, which is advantageous under corrosive and tribological conditions, is the objective [2]. In order to stabilize the ε-$Fe_3(N,C)_{1+x}$ phase and to avoid the formation of the γ'-Fe_4N phase within the compound layer, carbon-containing gas, such as CH_4, is admixed to nitrogen-rich plasmas. However, in addition to the positive effect of small CH_4 additions on the nitriding reaction, in the case of excess carbon, the undesired cementite Fe_3C phase is formed in the compound layer. Such a cementite formation within nitride layers is detrimental under tribological and fatigue loads and limits the process windows of PNC treatments using carbon-containing gases [3]. On the contrary, by using a solid-phase carbon source, Dalke et al. showed that on AISI 4140 steel, compound layers can form, which consist of nearly single-phase ε-$Fe_3(N,C)_{1+x}$ without

Fe_3C formation [4]. The solid-phase carbon material serves as a chemical source for carbon due to plasma-surface-interactions, forming HCN and various volatile hydrocarbons, such as C_2H_2, CH_4, C_2H_6, and CH_3 [5]. The mechanism known as chemical sputtering is characteristic for plasma-discharged carbon materials [6]. Besides hydrocarbons and HCN, NH_3 is formed from the N_2-H_2 precursor gas and CO from oxygen leakage [7]. In a comparative spectroscopic laboratory study, Hamann et al. [8] showed that on plasma-discharged surfaces the use of a carbon-fiber reinforced carbon (CFC) cathode increased the concentrations of carbon-containing species, such as HCN and C_2H_2, in the resulting process gas by more than one order of magnitude, compared to a steel material with methane gas addition. As a result of this finding, the concept of using a solid-carbon source for nitrocarburizing is implemented for the active screen (AS) technology by replacing the steel screen with a carbon screen made of CFC [9]. Analogously for the upscaled active screen plasma nitriding (ASPN) process, the capability of the carbon cathode was tested. Thereby, the concentrations of highly reactive plasma products were measured as functions of various process parameters, such as the power applied to the carbon screen, nitrogen-hydrogen ratio of the feed gas, pressure, and gas flow [7].

In addition to spectroscopic evidence of the improved reactive gas composition, various material studies show the possibilities of surface modification, using austenitic stainless steels as an example. Thereby, a significantly extended process window for a successful nitrocarburizing process was revealed. In particular, the nitrogen-hydrogen ratio [10] and the bias power at the steel components to be treated [11], as well as the power applied to the AS [12], were identified as factors influencing the resulting steel surface modifications. However, it was also demonstrated that the carbon-containing fraction within the resulting process gas can be varied only within small limits by lowering the plasma power at the carbon screen [12]. In order to exploit the possibilities of the extended process window of AS plasma nitrocarburizing (ASPNC) using a carbon AS for plain carbon and low-alloy steels, further concepts of process control and related parameters influencing the process itself need to be investigated. For instance, a conceivable option to affect the concentration of the carbon-containing fraction of the process gas, and, consequently, the carburizing potential, is the additional admixture of oxygen-containing gases to the nitrogen-hydrogen feed gas. For conventional plasma nitrocarburizing treatments using gaseous carbon precursors, such as CO_2, a positive effect of the oxygen-containing gas was reported [13,14]. However, the effect of an oxygen admixture to the nitrogen-hydrogen plasma of an ASPN process operating with a solid-phase carbon source on the resulting process gas composition, as well as the material response, have not yet been investigated. In addition, no long-term spectroscopic measurements accompanying the full duration of a material treatment are available. Especially in the context of an oxygen addition to the nitrogen-hydrogen feed gas, long-term spectroscopic gas diagnostic measurements can provide information on the stability of the process gas composition within the plasma-assisted process.

In this work, the effect of oxygen admixtures by applying O_2 and CO_2 additions to the N_2-H_2 feed gas was investigated within an industrial-scale cold-wall ASPN reactor. The main focus was to reduce the concentrations of carbon-containing reactive species within the resulting process gas in a controlled way. The resulting process gas composition's dependence on an oxygen admixture to the N_2-H_2 feed gas during short-term process cycles was measured by infrared laser absorption spectroscopy (IRLAS). The time-dependent developments of species concentrations were monitored in situ by IRLAS without and with an oxygen admixture during a nitrocarburizing material treatment of ARMCO® iron. The effect of an oxygen addition on the compound layer formation and the corresponding diffusion depth of nitrogen and carbon were revealed. The study aims to contribute to the understanding of the mechanisms of plasma-based nitrocarburizing processes and the interaction of the process gas atmosphere and the material reaction.

2. Materials and Methods

In an ASPN reactor, the influence of oxygen addition on the development of resulting process gas species was investigated. ASPN experiments using an AS made of CFC were performed in an industrial-scale cold-wall vacuum reactor with a reactor volume of approximately 1 m^3. A model probe—an assembly of connected rings—was placed in the center of the reactor and cathodically biased, cf. [15]. A resulting, so-called bias plasma was maintained at an applied power of 850 W. The diagnostic path for spectroscopy was located throughout the rings; the respective assembly was reported in detail in [15]. By IRLAS, the concentrations of seven molecular species, CH_4, C_2H_2, HCN, NH_3, CO, CO_2, and H_2O, were measured as functions of the level of O_2 and CO_2 admixture for a starting feed gas mixing ratio of N_2:H_2 = 9:1. While the fraction of O_2 and CO_2 was stepwise increased from 0 to 10% of the total gas flow, the fraction of nitrogen was correspondingly decreased from 90 to 80% to maintain a constant hydrogen fraction of 10% in the constant total gas flow of Φ = 80 slh. It must be noted that the gas-mixing station was only equipped with an Ar mass flow controller, through which O_2 and CO_2 were introduced. The quantity was determined via manufacturer-provided conversion factors. Therefore, there may have been small deviations of the real gas fractions, compared to the nominal concentrations. The pressure was set to 3 mbar. The experiments were performed in such a way that the parameter set of the nitrogen-hydrogen-oxygen gas mixture was adjusted and kept constant for about 20 min, and then the IRLAS measurement was performed before the next gas mixture was set. Details of the IRLAS measurements method can be found in [16,17]. In Table 1, a list of detected species and their spectral positions, line strengths, and limits of detection are compiled.

Table 1. Species, spectral positions, room temperature line strengths, used for IRLAS measurements and their estimated limits of detection. The laser source for the given spectral position is denoted with a Q for EC-QCL (external-cavity quantum cascade lasers) and a T for TDL (lead salt tunable diode laser) sources, respectively. Data taken from the HITRAN database [18].

Species	Spectral Position (cm^{-1})	Absorption Line Strength (cm^{-1}/molecules cm^{-2})	Limit of Detection (molecules cm^{-3})	Ref.
$CH_4^{(Q)}$	1356.4868	1.784×10^{-20}	2×10^{13}	[19]
$CH_4^{(Q)}$	1356.5974	1.190×10^{-20}	2×10^{13}	[19]
$NH_3^{(Q)}$	1388.0552	2.726×10^{-22}	2×10^{14}	[20]
$NH_3^{(Q)}$	1767.5181	6.090×10^{-21}	2×10^{13}	[20]
$H_2O^{(Q)}$	1387.9337	8.769×10^{-23}	5×10^{14}	[18]
$H_2O^{(Q)}$	1388.3483	9.843×10^{-24}	2×10^{15}	[21]
$H_2O^{(Q)}$	1781.9619	1.167×10^{-21}	1×10^{14}	[21]
$C_2H_2^{(Q)}$	1356.8305	5.899×10^{-22}	5×10^{14}	[22]
$C_2H_2^{(Q)}$	1356.8881	8.920×10^{-21}	2×10^{13}	[22]
$HCN^{(Q)}$	1356.9389	4.636×10^{-23}	4×10^{14}	[23]
$HCN^{(Q)}$	1388.3225	3.592×10^{-22}	1×10^{14}	[24]
$CO^{(T)}$	2150.3409	1.840×10^{-21}	2×10^{11}	[25]
$CO^{(T)}$	2150.8560	1.826×10^{-19}	2×10^{13}	[25]
$CO_2^{(T)}$	606.2771	2.713×10^{-21}	5×10^{13}	[5]

Since the short-time gas-diagnostic measurements are always to be considered as a snapshot, no conclusions can be drawn from them regarding the long-term trends of the concentrations of major reaction products in the plasma-assisted process. Therefore, ASPN treatments of ferrous samples with concurrent time-dependent LAS measurements were conducted for both an admixture of 6% O_2 relative to the total nitrogen-hydrogen gas flow and without oxygen admixture.

For the material treatment, the system was evacuated and heated up by the glow discharge at the carbon AS to 510 °C (783 K) at 1.5 mbar in an hydrogen-argon atmosphere

(H_2:Ar = 3:1) at a total flow rate of 60 slh. After reaching the target temperature, the target gas composition was set to 84% N_2, 10% H_2, and 6% O_2 and 87% N_2, 10% H_2, and 3% O_2 with a total gas flow rate of 80 slh. For the reference treatment without O_2, the gas composition was set to 90% N_2, and 10% H_2. The measurements were performed at a temperature of 540 °C (813 K) at a constant pressure of 3 mbar for a treatment duration of 8 h followed by a cooling step in pure H_2 (Φ = 20 slh) until room temperature was reached. The power at the carbon AS during the treatment time was approximately 6 kW. Spectroscopic sampling of the current process gas composition occurred approximately every 20 min for the 8 h duration of an ARMCO® iron specimens' treatment. Therefore, 15 mm × 15 mm specimens were cut out of a 2 mm thick plate. Before the process, the samples' surfaces were polished to 1 µm surface finishing, cleaned in ethanol, and placed in the center of the vacuum reactor.

The formed compound layers were analyzed by glow discharge optical emission spectroscopy (GDOES) on a LECO SDP 750 spectrometer in order to quantify the element concentrations of nitrogen and carbon as well as their diffusion depths, and to examine the nitride layers with respect to a possible oxygen enrichment. Cross-sections of the treated samples were nickel-plated, metallographically prepared, and etched with sodium picrate etchant. Images of the compound layers were obtained with an optical microscope Carl Zeiss Neophot 30 equipped with a JVC TK C1381 CCD-camera. Furthermore, structural analyses of the nitrided layers were carried out by X-ray diffraction (XRD) in conventional θ-2θ Bragg-Brentano symmetric configuration using a SEIFERT-FPM URD6 (SEIFERT-FPM) diffractometer with a scan rate of 0.01°/min and 2θ angle ranging from 20° to 150°. The diffractometer was equipped with a sealed X-ray tube with a Co anode (Co-$K_{\alpha 1}$: λ = 1.78897 Å) operating at a voltage of U = 40 kV and a current of I = 30 mA. The Rietveld refinement method was applied to determine the quantitative phase composition.

3. Results

3.1. Spectroscopic Investigations

Figure 1 presents the concentrations of seven detectable reaction products of the ASPNC process. The level of the O_2 or CO_2 admixture is given as a fraction of the feed gas on the x-axis, as well as an equivalent concentration as a dashed line in the respective figure.

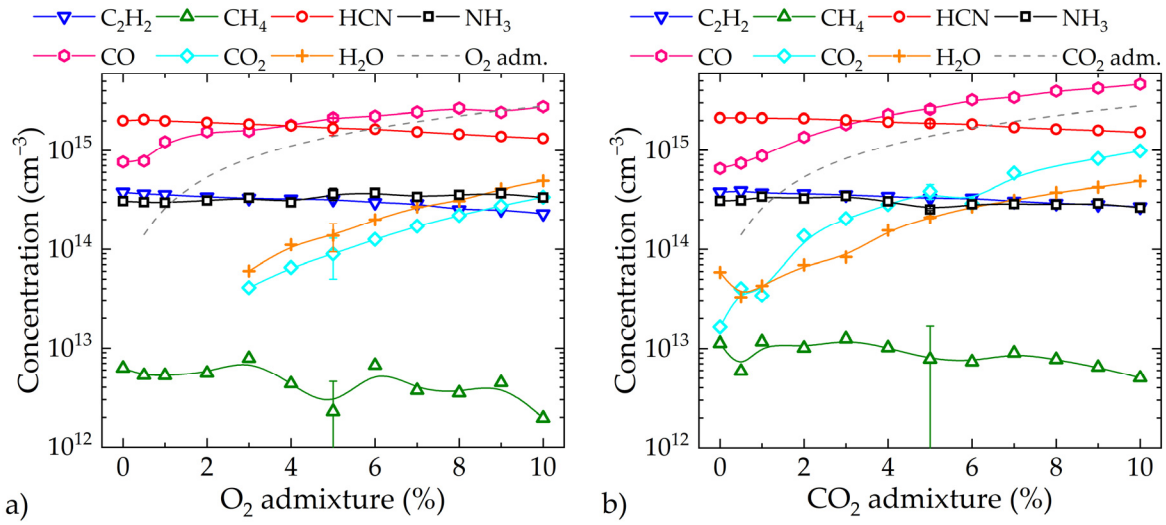

Figure 1. Concentrations of C_2H_2, CH_4, HCN, NH_3, CO, CO_2, and H_2O as functions of (**a**) O_2 and (**b**) CO_2 admixture. T = 540 °C, N_2 + O_2 = 90% or N_2 + CO_2 = 90%, H_2 = 10%, P_{AS} = 6.0 kW.

In the pure nitrogen-hydrogen feed gas, i.e., without admixture of O_2 or CO_2, HCN is the most abundant reaction product, followed by CO, C_2H_2, NH_3, and CH_4. Oxygen was present due to impurities in the technical precursor gas, leakage in the vacuum reactor,

or sources from the steel surface of the model probe, and was primarily detected after its reaction to CO.

Both O_2 and CO_2 were dissociated in the reactor under the release of oxygen, which can react to further chemical compounds. As a result, the fundamental dependencies of the species concentrations towards the oxygen-containing precursor gases were comparable. For CO_2, the degree of dissociation was about 74%. This reduces the concentrations of reactive chemical compounds, such as HCN or C_2H_2. Additionally, the high affinity of hydrogen to oxygen led to the formation of H_2O. By increasing the O_2 or CO_2 admixture in the nitrogen-hydrogen feed gas, the concentrations of the oxygen-containing species were monotonically increased, and more of the sputtered carbon reacted to form stable species CO and CO_2, and did not participate in formation of hydrocarbons and CN-species. Therefore, concentrations of HCN, CH_4, and C_2H_2 were monotonically decreased, while NH_3 was slightly increased due to the proposed reaction paths as follows [26]:

$$2 \cdot C_xH_y + 0.5 \cdot (4x + y) \cdot O_2 \rightarrow 2x \cdot CO_2 + y \cdot H_2O \quad (1)$$

$$HCN + 0.5 \cdot O_2 \rightarrow HNCO \quad (2)$$

$$HNCO + H_2O \rightarrow NH_3 + CO_2 \quad (3)$$

As an intermediate product, HCNO decomposed to NH_3 and CO_2. At higher oxygen contents above 7%, CO becomes the species with the highest concentration. In addition, more hydrogen formed H_2O, resulting in a decreased NH_3 concentration.

The normalized oxygen distribution in the reactive species CO, CO_2, and H_2O is shown in Figure 2 in which 100% corresponds to the amount of oxygen that was fed into the reactor.

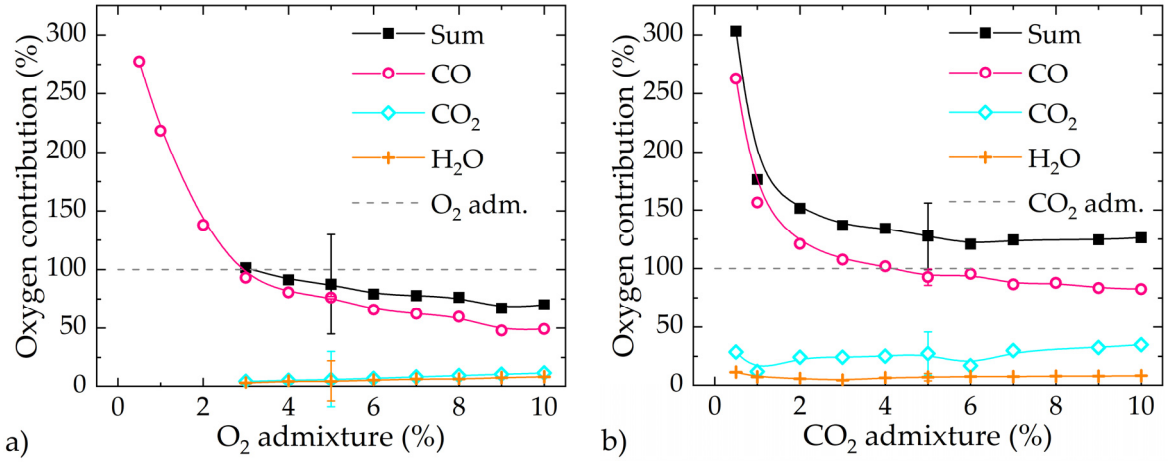

Figure 2. Normalized atomic oxygen contributions of the oxygen-containing species (CO, CO_2, and H_2O) and their sum related to the oxygen content in the precursor gas for (**a**) O_2 and (**b**) for CO_2. T = 540 °C, $N_2 + O_2$ = 90% or $N_2 + CO_2$ = 90%, H_2 = 10%, P_{AS} = 6.0 kW.

For both O_2 and CO_2, at a low flow rate, it is apparent that the sum of all oxygen-containing species is well above 100%, which can be attributed to the leakage and contamination of reactor parts only. As a result, more oxygen is present and bonds preferentially as CO. As Figure 2a shows, H_2O and CO_2 were detectable only at O_2 admixtures larger than 3%, with their concentrations remaining close to their limits of detection even at high levels of admixture. The sum of the above-mentioned oxygen-containing species falls below 100% for more than 3% O_2 admixture. The likely reason is the degree of dissociation of oxygen and the contamination of the reactor. With an increased O_2 concentration, leakage becomes less important, whereas the degree of dissociation of O_2 might be regarded as relatively constant or even decreasing resulting in saturation at about 70%. However, no statement can be made about the degree of dissociation by means of IRLAS, since O_2 cannot

be measured spectroscopically in the infrared range. However, it is also conceivable that other undetected oxygen-containing species, like N_2O or NO_x, were formed.

For CO_2, Figure 2b shows that the normalized sum of all oxide species is well above 100% for all admixtures. In contrast to the O_2 admixture, CO_2 is measurable by means of IRLAS and can therefore be included in the consideration. Overestimating the value above 100% could be related to measurement inaccuracies of the spectroscopic measurements and the CO_2 flow through Ar mass flow controllers, which may have slightly underestimated the CO_2 flow rate. However, this does not affect the relationship between the species being formed to an exaggerated extent. The percentage values must accordingly be regarded as slightly overestimated. Unlike in the case of O_2 admixture, the carbon in CO can have two possible sources. On the one hand, CO may form by the CO_2 dissociation itself, and on the other hand, oxygen is released by the dissociation of CO_2, which in turn reacts with the carbon from the AS to CO. H_2O was formed accordingly. The content of H_2O is almost constant around approx. 10%. Based on the results, it can be concluded that oxygen influenced the concentrations of species that are responsible for carburizing potentials. O_2 and CO_2 can be used in order to reduce the concentrations of HCN and C_2H_2 in analogy to the effect of a reduction of the power at the carbon surface.

3.2. In Situ Gas Analysis during Process Monitoring

In the following analysis, the long-term trends of the concentrations of detectable reactive species in the process with and without oxygen were investigated. During the process, the concentrations of the main products HCN, NH_3, C_2H_2, and CH_4 were monitored with an average time resolution of Δt = 20 min. Figure 3 presents the results of this long-term measurement, both for the process with a 6% oxygen admixture (red line) and without (black line).

As a result of the O_2 addition, the concentrations of the carbon-containing species (HCN, C_2H_2, CH_4) were reduced significantly while the concentration of NH_3 was increased. With progressing treatment time, the concentrations of HCN and C_2H_2 slightly decreased, while NH_3 and CH_4 were almost unaffected. This trend can be explained by the temperature balance and the resulting AS power in the ASPN reactor. Since the reactor is water-cooled, there is balance between the energy supplied by the AS and the energy dissipated at the cooled wall. This equilibrium, however, is approached over time and was not initially established. Thus, at the beginning of the process, the AS power was higher and decreased over time. Since the production rates of the species generated at the AS show a power dependency, the concentrations of the species changed with time and decreased steadily for HCN and C_2H_2. Nevertheless, the conditions during the material treatment are relatively stable in terms of the concentrations of the detected gas species.

3.3. Surface Modification of ARMCO® Iron

Figure 4a presents the resulting concentration-depth profiles of N, C, and O as determined by GDOES.

The incorporation of oxygen into the material is independent of the admixture of oxygen-containing precursors within the margin of error. Consequently, oxygen was not preferably introduced into the surface despite its higher concentration in the vacuum reactor. However, oxygen had an indirect influence on the layer modification, since the nitrogen and carbon profiles were significantly changed by the addition of oxygen.

The maximum concentration of nitrogen reached up to approx. 20 wt% and was not significantly affected by the O_2 addition. However, the depth profile changed, and more nitrogen diffused into the surface with the admixture of O_2 in the feed gas. Thus, the diffusion depth of nitrogen increased from approximately 21 µm to approximately 28 µm, resulting in a significantly thicker compound layer. At the same distance from the surface, a higher concentration of nitrogen was present for 6% O_2. No significant increase in the local nitrogen concentration at 3% O_2 was detected. In contrast, the carbon content integrated over the depth was almost identical in all cases. However, the local carbon maximum was

reduced from 0.5 wt% to 0.4 and 0.3 wt% and the area of carbon enrichment was pushed further towards the bulk material.

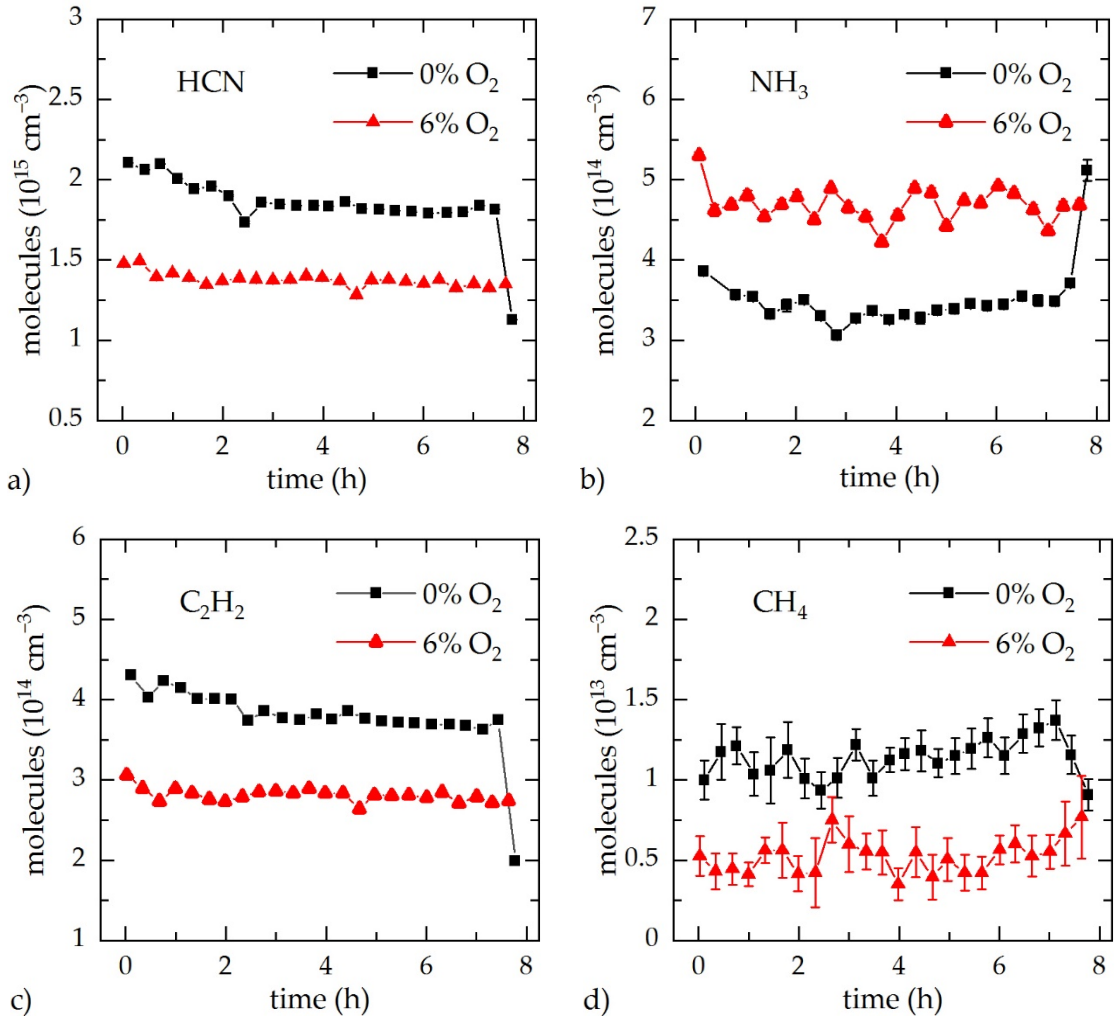

Figure 3. Monitored concentrations of (**a**) HCN, (**b**) NH_3, (**c**) C_2H_2, and (**d**) CH_4 during the treatment in the industrial scale ASPN reactor with (red) and without (black) the admixture of 6% O_2 in the N_2-H_2 feed gas. T = 540 °C, N_2 + O_2 = 90%, H_2 = 10%, P_{AS} = 6.0 kW.

In Figure 4b nickel-plated cross sections of the resulting surface layers with different O_2 concentrations are presented. The layers consisted mainly of a sandwich-like structure with columnar ε-$Fe_3(N,C)_{1+x}$ grains and a thin layer of γ′-Fe_4N at the interspace of the compound layer to the bulk caused by decreased local nitrogen concentrations. From the micrographs, it can be concluded that the compound layer thickness as well as the porosity was increased by the addition of oxygen.

The phase formation as a function of the oxygen content was studied with X-ray diffraction. In Figure 5a, the X-ray diffraction profiles of the untreated ARMCO® iron and treated specimens are given.

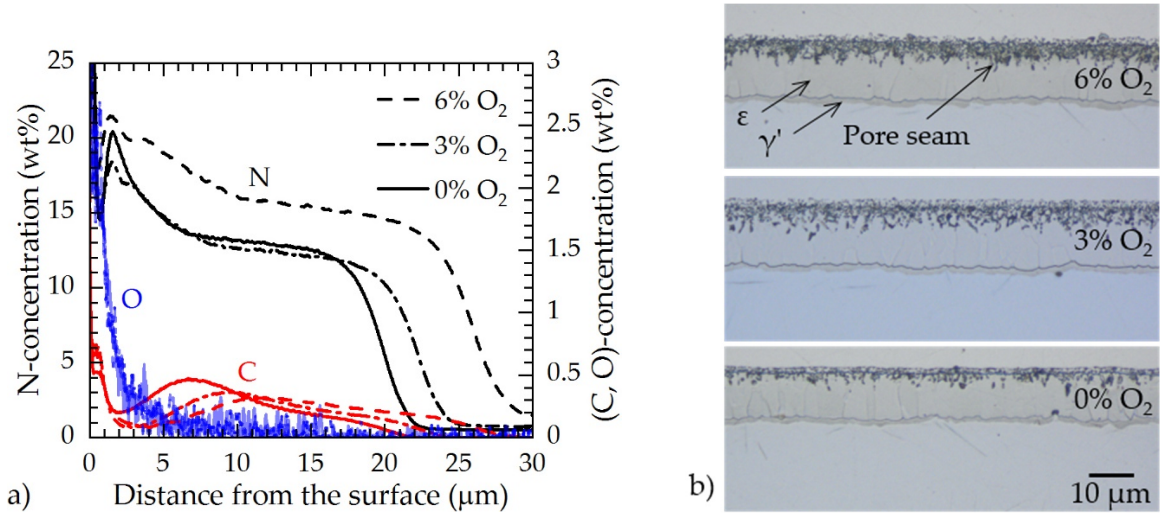

Figure 4. (**a**) Element concentration-depth profiles of nitrogen, carbon, and oxygen of the ARMCO® iron samples treated with 6% (dashed curves), with 3% (dash-dot curves), and without (solid curves) the usage of O_2 in the N_2-H_2 feed gas; (**b**) cross sections of compound layers formed on ARMCO® iron for different O_2 concentrations; sodium picrate etchant. T = 540 °C, N_2 + O_2 = 90%, H_2 = 10%, P_{AS} = 6.0 kW.

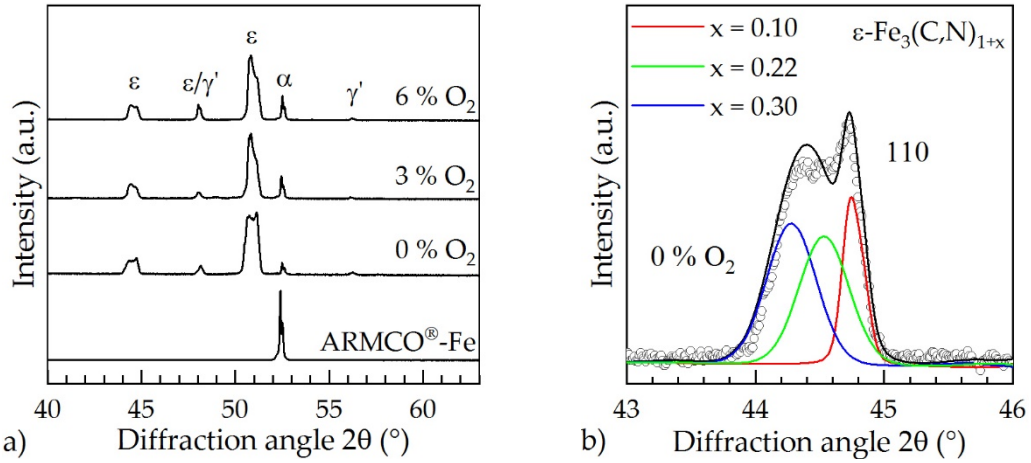

Figure 5. (**a**) X-ray diffraction patterns using Co-Kα radiation; (**b**) peak analysis of the ε(110) peak at 0% oxygen. Values for x estimated from [27]. T = 540 °C, N_2 + O_2 = 90%, H_2 = 10%, P_{AS} = 6.0 kW.

The compound layer on top of bcc α-Fe consists of γ′-Fe_4N (cubic, space group $Pm\bar{3}m$) and a derivative of the ε-Fe_3N_{1+x} phase (hexagonal, space group $P6_322$). It is remarkable to note, that the peaks of ε-Fe_3N_{1+x} in Figure 5a (except for 00l lines) are atypically broadened. The atypical broadening of the peaks results from the overlapping of a number of ε-$Fe_3(N,C)_{1+x}$ peaks being slightly mutually displaced. The displacement is a result of changes in the a lattice parameter induced by the solution of C in ε-Fe_3N_{1+x} to form ε-$Fe_3(N,C)_{1+x}$ [28] and the total interstitial content (C + N) [29]. It is assumed that the total (C + N) interstitial content provides the largest effect for the lattice parameter expansion [28]. A detailed investigation of the ε-$Fe_3(N,C)_{1+x}$ peak profiles by means of a detailed line-profile analysis, in order to extract lattice parameter distributions, is beyond the scope of this report. Instead, Rietveld refinement was used to estimate the average phase composition of the compound layer.

The quantitative phase composition determined by means of the Rietveld method indicated that the compound layers were mostly made of ε-$Fe_3(N,C)_{1+x}$ (~ 95%) and small fractions of γ′-Fe_4N (~ 5%). In order to mimic the complicated shape of the broadened peaks of ε-$Fe_3(N,C)_{1+x}$, three phases ε-Fe_3N_{1+x} (see Table 2) have been used with slightly

different *a* lattice parameters but identical *c* lattice parameters. The latter is justified by the absence of the atypical peak broadening for 00l reflections. Line-width parameters were also refined. As both the total interstitial content (C + N) and the interstitial C/N ratio change the unit cell dimensions of ε-$Fe_3(N,C)_{1+x}$ [28], it is impossible to derive the exact composition range of the extremes of the lattice parameters from the current sample and data set.

Table 2. Structure, lattice parameters, and the quantitative fraction (relative and absolute) of ε-$Fe_3(N,C)_{1+x}$ (x = 0.10, 0.22, 0.30; values for *x* estimated from [27]) determined by X-ray diffraction and Rietveld method.

		$Fe_3(N,C)_{1+x}$ (x = 0.10)		
Oxygen (vol%)	**a (nm)**	**c (nm)**	**rel. (vol%)**	**abs. (vol%)**
0	0.4716 (3)	0.4407 (1)	13	12 ± 2
3	0.4713 (2)	0.4406 (1)	27	25 ± 2
6	0.4713 (2)	0.4409 (1)	26	24 ± 2
		$Fe_3(N,C)_{1+x}$ (x = 0.22)		
Oxygen (vol%)	**a (nm)**	**c (nm)**	**rel. (vol%)**	**abs. (vol%)**
0	0.4738 (1)	0.4407 (1)	41	39 ± 3
3	0.4736 (2)	0.4406 (1)	35	32 ± 3
6	0.4734 (2)	0.4409 (1)	36	33 ± 3
		$Fe_3(N,C)_{1+x}$ (x = 0.30)		
Oxygen (vol%)	**a (nm)**	**c (nm)**	**rel. (vol%)**	**abs. (vol%)**
0	0.4764 (1)	0.4407 (1)	46	43 ± 4
3	0.4753 (2)	0.4406 (1)	37	34 ± 3
6	0.4754 (2)	0.4409 (1)	38	35 ± 3

Additionally, a possible incorporation of oxygen into the carbonitride and its effect on the lattice parameter of a hypothetical ε-$Fe_3(N,C,O)_{1+x}$ cannot be deduced from the data. However, the absence of Fe-oxide phases in the XRD patterns may support the existence of an ε-$Fe_3(N,C,O)_{1+x}$ but can also have different causes, such as a very thin oxide surface layer being below the detection limit for XRD or the formation of amorphous oxides, e.g., as a layer at the surface.

Given the GDOES results (Figure 4a), an alteration of the C/N ratio with layer depth (and eventually also the variation in the total interstitial content (C + N)) can be safely assumed and is, thus, made responsible for the observed peak broadening due to the lattice parameter changes. The penetration depth of the X-rays is in the order of the compound layer thickness. The lattice parameters and the relative phase fractions of the three phases used in Rietveld refinement of the XRD patterns shown in Figure 5a are compiled in Table 2. The determined lattice parameters allow for categorizing the used ε-Fe_3N_{1+x} phases in low-, medium- and high-interstitial bearing ε-Fe_3N_{1+x} (x = 0.10, 0.22, 0.30) (Figure 5b), where N has to be replaced here with (N,C), with the aid of ICDD-PDF4 database entries (see Table 2). Here, the values of *x* have been selected from [27] as the closest matches for the lattice parameters determined for the present samples.

The mutual changes of the lattice parameters as a function of the oxygen content in the reactive atmosphere are all within experimental error and thus do not generate a systematic trend. Contrarily, the relative volume fractions of ε-$Fe_3(N,C)_{1+x}$ indicate that the presence of oxygen in the reactive atmosphere promotes lower total (C + N) interstitial contents. This effect is not directly reflected in Figure 5a because it is camouflaged by an increase in the peak width (increase in lattice microstrain/decrease in crystallite size) of the low-interstitial ε-$Fe_3(N,C)_{1+x}$ phase upon addition of oxygen to the reactive atmosphere. This observation is concomitant with the occurrence of a thicker pore seam at the compound layer surface (cf. Figure 4b), but a direct connection of these two observations cannot be established based on the presented/available data.

4. Discussion

The feasibility of an oxygen admixture to an N_2-H_2 plasma in an ASPN process using an CFC active screen was investigated. Additions of O_2 and CO_2 significantly reduced the concentrations of hydrocarbons and CN-species, but increased the CO, CO_2, and H_2O concentrations. Furthermore, the NH_3 concentration was increased since more sputtered carbon formed CO. As a result, more unbound hydrogen and nitrogen were freely available in the plasma to form NH_3. At very high oxygen concentrations, however, the hydrogen was oxidized to H_2O and, therefore, no longer available for the formation of NH_3, which, in turn, decreased the concentration in the process.

Furthermore, long-term in situ monitoring has shown negligible trends in the concentrations of major reaction products over the typical duration of ASPNC treatments. Without oxygen addition, it was found that there was a non-negligible oxygen content in the reactor, which is always present during plasma processes due to the use of technical gases, leakage and the contamination of surfaces. The predominant oxidation product was CO.

As the admixture of oxygen-containing species impacted the concentration of reactive species in the process, we further studied its effect on the material treatment results. The addition of oxygen progressively lowered the concentration of HCN and C_2H_2; however, the formed species (CO, CO_2) are known to facilitate carburization of metal surfaces in conventional PNC.

During the material treatment of ARMCO® iron with an admixture of 3% and 6% O_2, respectively, no excessive oxygen enrichment was detected in the nitrided layer. In contrast, the nitrogen content in the compound layer increased significantly, which increased both the concentration and the diffusion depth, resulting in a thicker compound layer and higher porosity. The integral carbon content over the depth was almost identical in all cases. However, the maximum carbon concentration in the compound layer (0.5 wt%) was lowered (0.4 and 0.3 wt%) and shifted further towards the base material in the case of the O_2 admixture. Both effects could ensure that the potential formation of cementite in plain carbon or low-alloyed steels is reduced by increased nitrogen and reduced carbon activity. Future in-depth optical emission spectroscopy investigations are required to gain more insights on this.

The compound layer on ARMCO® iron consisted mainly of ε-$Fe_3(N,C)_{1+x}$ and small fractions of γ'-Fe_4N and was not significantly changed with regards to the phase composition.

Compared to conventional plasma nitriding, where the formation of oxide layers above a critical oxygen concentration hinders nitrogen and carbon diffusion, high oxygen contents in the reaction gas of ASPNC processes operating a solid carbon precursor, such as CFC, do not negatively affect the material treatment. Rather, the positive changes on the plasma chemistry are to be emphasized. The reason could be due to the high carbon concentration and species concentration in the plasma. Oxygen is preferentially bound as CO and, thus, obviously does not tend to form an oxide layer. However, other reactive species, such as HCN, could ensure that a newly formed oxide layer is removed directly, so that a thick and continuous oxide layer cannot generate.

5. Conclusions

In this work, the impact of two oxygen-containing precursor gases, O_2 and CO_2, on a plasma nitrocarburizing process using an active screen made of carbon-fiber reinforced carbon was investigated in order to control and adjust the carburizing efficiency, i.e., the carbon potential, of the resulting process gas composition. With increasing oxygen addition to the N_2-H_2-plasma, a reduction of the concentrations of HCN and C_2H_2 was measured by laser absorption spectroscopy. In contrast, oxygen-containing species, such as CO, CO_2, and H_2O as well as NH_3, were slightly increased. The long-term measurements at the vacuum reactor demonstrated that the atmosphere can be regarded as nearly constant over a long period of time.

Despite enhanced oxygen concentrations within the process gas, no significant oxygen enrichment was observed in the compound layer of ARMCO® iron. However, the diffusion depth of nitrogen and carbon increased significantly. This effect can allow further modification of the compound layers of plain carbon or low-alloyed steels during active screen plasma nitrocarburizing.

Author Contributions: Conceptualization, J.B., A.P., A.D.; methodology, A.P., A.D.; validation, formal analysis, H.B., J.R.; investigation, A.P., J.B., C.S.; resources, H.B., J.R.; data curation, A.P., J.B.; writing—original draft preparation, J.B., A.D.; writing—review and editing, C.S., A.D., H.B.; visualization, A.P., J.B.; supervision, H.B., J.-P.H.v.H.; project administration, H.B., J.R.; funding acquisition, J.R., H.B. All authors have read and agreed to the published version of the manuscript.

Funding: This research was funded by the Deutsche Forschungsgemeinschaft (DFG, German Research Foundation: 289846720) (BI 418/31-2; RO 2202/10-2). Open Access Funding by the Publication Fund of the TU Bergakademie Freiberg.

Acknowledgments: The authors thank Igor Burlacov (now at G + M Vacutherm Härterei- und Oberflächentechnik GmbH) for the implementation of the experiments and Stephan Hamann (now at CHEPLAPHARM Arzneimittel GmbH) for the implementation of LAS measurements.

Conflicts of Interest: The authors declare no conflict of interest.

References

1. Mittemeijer, E.; Somers, M.A.J. (Eds.) *Thermochemical Surface Engineering of Steels*; Elsevier: Amsterdam, The Netherlands, 2015; ISBN 9780857095923.
2. Bell, T.; Sun, Y.; Suhadi, A. Environmental and technical aspects of plasma nitrocarburising. *Vacuum* **2000**, *59*, 14–23. [CrossRef]
3. Basso, R.L.O.; Figueroa, C.A.; Zagonel, L.F.; Pastore, H.O.; Wisnivesky, D.; Alvarez, F. Effect of Carbon on the Compound Layer Properties of AISI H13 Tool Steel in Pulsed Plasma Nitrocarburizing. *Plasma Process. Polym.* **2007**, *4*, S728–S731. [CrossRef]
4. Dalke, A.; Burlacov, I.; Spies, H.-J.; Biermann, H. Use of a solid carbon precursor for DC plasma nitrocarburizing of AISI 4140 steel. *Vacuum* **2018**, *149*, 146–149. [CrossRef]
5. Puth, A.; Hamann, S.; Kusýn, L.; Burlacov, I.; Dalke, A.; Spies, H.-J.; Biermann, H.; Röpcke, J. Spectroscopic investigations of plasma nitrocarburizing processes using an active screen made of carbon in a model reactor. *Plasma Sources Sci. Technol.* **2018**, *27*, 75017. [CrossRef]
6. Bystrov, K.; Morgan, T.W.; Tanyeli, I.; de Temmerman, G.; van de Sanden, M.C.M. Chemical sputtering of graphite by low temperature nitrogen plasmas at various substrate temperatures and ion flux densities. *J. Appl. Phys.* **2013**, *114*, 133301. [CrossRef]
7. Puth, A.; Kusýn, L.; Pipa, A.V.; Burlacov, I.; Dalke, A.; Hamann, S.; van Helden, J.H.; Biermann, H.; Röpcke, J. Spectroscopic study of plasma nitrocarburizing processes with an industrial-scale carbon active screen. *Plasma Sources Sci. Technol.* **2020**, *29*, 35001. [CrossRef]
8. Hamann, S.; Burlacov, I.; Spies, H.-J.; Biermann, H.; Röpcke, J. Spectroscopic investigations of plasma nitriding processes: A comparative study using steel and carbon as active screen materials. *J. Appl. Phys.* **2017**, *121*, 153301. [CrossRef]
9. Burlacov, I.; Hamann, S.; Spies, H.-J.; Dalke, A.; Röpcke, J.; Biermann, H. A Novel Approach of Plasma Nitrocarburizing Using a Solid Carbon Active Screen—A Proof of Concept. *HTM J. Heat Treat. Mater.* **2017**, *72*, 254–259. [CrossRef]
10. Dalke, A.; Burlacov, I.; Hamann, S.; Puth, A.; Böcker, J.; Spies, H.-J.; Röpcke, J.; Biermann, H. Solid carbon active screen plasma nitrocarburizing of AISI 316L stainless steel: Influence of N_2-H_2 gas composition on structure and properties of expanded austenite. *Surf. Coat. Technol.* **2019**, *357*, 1060–1068. [CrossRef]
11. Jafarpour, S.; Puth, A.; Dalke, A.; Böcker, J.; Pipa, A.; Röpcke, J.; van Helden, J.-P.H.; Biermann, H. Solid carbon active screen plasma nitrocarburizing of AISI 316L stainless steel in cold wall reactor: Influence of plasma conditions. *J. Mater. Res. Technol.* **2020**, *9*, 9195–9205. [CrossRef]
12. Böcker, J.; Puth, A.; Dalke, A.; Röpcke, J.; van Helden, J.-P.H.; Biermann, H. Influence of the Active Screen Plasma Power during Afterglow Nitrocarburizing on the Surface Modification of AISI 316L. *Coatings* **2020**, *10*, 1112. [CrossRef]
13. Haruman, E.; Bell, T.; Sun, Y. Compound layer characteristics resulting from plasma nitrocarburising in atmospheres containing carbon dioxide gas additions. *Surf. Eng.* **1992**, *8*, 275–282. [CrossRef]
14. Hamann, S.; Börner, K.; Burlacov, I.; Hübner, M.; Spies, H.-J.; Röpcke, J. Spectroscopic studies of conventional and active screen N_2–H_2 plasma nitriding processes with admixtures of CH_4 or CO_2. *Plasma Sources Sci. Technol.* **2013**, *22*, 55022. [CrossRef]
15. Burlacov, I.; Börner, K.; Spies, H.-J.; Biermann, H.; Lopatik, D.; Zimmermann, H.; Röpcke, J. In-Situ monitoring of plasma enhanced nitriding processes using infrared absorption and mass spectroscopy. *Surf. Coat. Technol.* **2012**, *206*, 3955–3960. [CrossRef]
16. Hamann, S.; Börner, K.; Burlacov, I.; Spies, H.-J.; Röpcke, J. Spectroscopic diagnostics of active screen plasma nitriding processes: On the interplay of active screen and model probe plasmas. *J. Phys. D Appl. Phys.* **2015**, *48*, 345204. [CrossRef]

17. Hamann, S.; Börner, K.; Burlacov, I.; Spies, H.-J.; Strämke, M.; Strämke, S.; Röpcke, J. Plasma nitriding monitoring reactor: A model reactor for studying plasma nitriding processes using an active screen. *Rev. Sci. Instrum.* **2015**, *86*, 123503. [CrossRef]
18. Gordon, I.E.; Rothman, L.S.; Hill, C.; Kochanov, R.V.; Tan, Y.; Bernath, P.F.; Birk, M.; Boudon, V.; Campargue, A.; Chance, K.V.; et al. The HITRAN2016 molecular spectroscopic database. *J. Quant. Spectrosc. Radiat. Transf.* **2017**, *203*, 3–69. [CrossRef]
19. Ba, Y.A.; Wenger, C.; Surleau, R.; Boudon, V.; Rotger, M.; Daumont, L.; Bonhommeau, D.A.; Tyuterev, V.G.; Dubernet, M.-L. MeCaSDa and ECaSDa: Methane and ethene calculated spectroscopic databases for the virtual atomic and molecular data centre. *J. Quant. Spectrosc. Radiat. Transf.* **2013**, *130*, 62–68. [CrossRef]
20. Cottaz, C.; Kleiner, I.; Tarrago, G.; Brown, L.R.; Margolis, J.S.; Poynter, R.L.; Pickett, H.M.; Fouchet, T.; Drossart, P.; Lellouch, E. Line Positions and Intensities in the 2nu(2)/nu(4) Vibrational System of (14)NH(3) near 5–7 μm. *J. Mol. Spectrosc.* **2000**, *203*, 285–309. [CrossRef] [PubMed]
21. Toth, R.A. H_2O Linelist. Available online: https://mark4sun.jpl.nasa.gov/h2o.html (accessed on 3 August 2021).
22. Gomez, L.; Jacquemart, D.; Lacome, N.; Mandin, J.-Y. New line intensity measurements for 12C2H2 around 7.7μm and HITRAN format line list for applications. *J. Quant. Spectrosc. Radiat. Transf.* **2010**, *111*, 2256–2264. [CrossRef]
23. Maki, A.G.; Mellau, G.C.; Klee, S.; Winnewisser, M.; Quapp, W. High-Temperature Infrared Measurements in the Region of the Bending Fundamental of H12C14N, H12C15N, and H13C14N. *J. Mol. Spectrosc.* **2000**, *202*, 67–82. [CrossRef]
24. Maki, A.G.; Quapp, W.; Klee, S. Intensities of Hot-Band Transitions: HCN Hot Bands. *J. Mol. Spectrosc.* **2000**, *171*, 420–434. [CrossRef]
25. Coxon, J.A.; Hajigeorgiou, P.G. Direct potential fit analysis of the X1sigma+ ground state of CO. *J. Chem. Phys.* **2004**, *121*, 2992–3008. [CrossRef]
26. Kröcher, O.; Elsener, M. Hydrolysis and oxidation of gaseous HCN over heterogeneous catalysts. *Appl. Catal. B Environ.* **2009**, *92*, 75–89. [CrossRef]
27. Leineweber, A.; Jacobs, H.; Hüning, F.; Lueken, H.; Kockelmann, W. Nitrogen ordering and ferromagnetic properties of ϵ-Fe_3N_{1+x} ($0.10 \leq x \leq 0.39$) and ϵ-$Fe_3(N_{0.80}C_{0.20})_{1.38}$. *J. Alloys Compd.* **2001**, *316*, 21–38. [CrossRef]
28. Jack, K.H. Binary and Ternary Interstitial Alloys. II. The Iron-Carbon-Nitrogen System. *Proc. R. Soc. Lond.* **1948**, *195*, 41–55.
29. Jacobs, H.; Rechenbach, D.; Zachwieja, U. Structure determination of γ′-Fe4N and ϵ-Fe3N. *J. Alloys Compd.* **1995**, *227*, 10–17. [CrossRef]